Title Dynamic analysis of composite marine structures using full-field measurement techniques

Authors G Crammond, S W Boyd and J M Dulieu-Barton

Fluid structures interaction research group, Faculty of Engineering and the Environment, University of Southampton, Southampton, SO17 1BJ, UK

Synopsis Composite materials are increasingly used in structural applications within the marine industry. Due to the geometric complexity of marine structures, there is a practical requirement that they are assembled by joining smaller component pieces using either mechanical fasteners or adhesive bonding. In this paper Digital Image Correlation (DIC) is used to provide full-field analysis of the complex strain fields generated within an adhesively bonded composite single lap joint. Tests are undertaken quasi-statically and at high rate, demonstrating a significant change in the assembly response between laboratory testing conditions and dynamic loading events typical of the marine environment. The work demonstrates the potential of applying full-field experimental technique to provide detailed analysis of complex structural problems, typical of large marine structures.

Authors Biography George Crammond was awarded an MEng in Ship Science at the University of Southampton with a specialist theme in advanced materials. He was awarded a PhD from the University of Southampton in 2013 for his thesis titled 'Development of optical techniques for the experimental analysis of local stress and strain distributions in adhesively bonded composite joints'. In 2009 he was awarded the IMarEST Stanley Gray Fellowship to support his research.

Dr Stephen Boyd is a Senior Lecturer in Ship Science at the University of Southampton. He is a naval architect and his research interests focus around the application of composite materials in the maritime environment. He is investigator on a number of research council

projects including performance of fire retardant composite resins, damage tolerance of composites subject to high speed loading and the use of tailored composites for tidal turbine blades.

Janice Dulieu-Barton is a Professor of Experimental Mechanics and has worked in the field since 1989. She has published more than 250 papers on this and related topics. Professor Barton's primary research interest is in imaging. Applications include: damage analysis of composite/ sandwich/ textile materials, crack-tip stress studies and small scale full-field experimental stress analysis. She is a Fellow of the UK Institute of Physics, a Chartered Mechanical Engineer and associate editor of the international journal for experimental mechanics: Strain.

Introduction

The beneficial specific material properties of polymer composites is leading to their increased usage in the marine industry. The use of composites have been shown to offer structural weight savings up to 36% for a large 52m naval patrol vessel compared to a comparable steel hulled craft [1]. Through their use, lighter vessels experience operational and financial gains such as increased payload capacity and improved fuel consumption in addition to lowering the centre of gravity of the structure, producing better stability and sea keeping characteristics. However, the increasing size of marine structures makes it impractical for a single shot continuous moulding process to be employed, favouring the assembly of the vessel from a strengthened shell hull structure. Therefore joints are required either to assemble the composite structure from many smaller component parts or for the attachment of secondary strengthening support structure, as shown in Fig 1.

FIG 1

Joints present a significant design challenge to engineers as they inherently contain discontinuities in both geometry and material properties, generating complex stress and strain distributions. Mechanical fastenings such as rivets, screws and bolts are currently the most common joining mechanism used in industry. Their benefits include little surface preparation, cheap component costs and are relatively easy to assemble and dismantle, which is very important for the inspection, repair and maintenance of the structures [2–4].

The strength of mechanically fastened joints is provided by the non-slip frictional forces generated by contact between the adherend bearing surfaces. The mechanical fastener provides through-thickness reinforcement within the joint, forcing the bearing surfaces together, increasing the contact force between adherends and hence increasing the ultimate joint strength. The weak through-thickness properties of the composite material limits the pretension that can be applied to the fastener without damage [5], which inevitably reduces the contact between joint faces and hence the ultimate joint strength. Fretting damage between the metallic fastener and the composite is also a possibility [6] increasing joint compliance and decreasing the contact force between adherends. In addition the introduction of a hole to accept the fastener results in fibre discontinuity in the composite requiring the continuous fibres, in the vicinity of the hole, to carry more load. Ultimately mechanically fastened joints are heavy and time consuming to manufacture, conflicting the high strength and low weight benefits of composite materials. This provides the motivation for developing a better understanding of alternative joining techniques.

The main alternative to mechanical fastening is adhesive bonding. The adhesive between adherends forms a coherent structural layer chemically bonded between the adherend surfaces, across which load is transferred. Epoxy based adhesives are most commonly used in the marine industry due to their high strength, ease of application, good service temperature range, resistance to moisture and chemical attack, and ability to bond a variety of different substrate materials. The use of adhesive bonding provides a significant reduction in joint weight compared to mechanical fasteners [1], increasing the structural efficiency of the joint. Reductions in assembly time and part count, improving the ease of manufacture and reducing the cost of production, are also experienced. Some surface preparation is required during manufacture to clean the component surfaces, such that there is a good chemical compatibility between the adherend and the adhesive, which largely governs the bond strength.

Adhesive joint analysis

The discontinuous nature of both mechanically fastened and adhesive bonded joints creates significant through-thickness load transfer between components. Marine structures also experience high through-thickness loading from significant global bending and torsion loads in the structure. In the mechanically fastened joint, the fastener provides reinforcement and strength between adherends in the through-thickness direction. In contrast, the through-thickness load transfer in the adhesive joint is dependent on the chemical bond between the adhesive and the adherend surface. Bonded composite joints provide a difficult problem as composites, though strong in the direction of the fibres, are weak normal to the fibre direction, where their strength is dominated by the mechanical properties of the brittle polymer matrix. Their weak through-thickness properties, and the relatively high through-thickness loading across the discontinuity, make the laminate susceptible to the initiation of interlaminar cracks leading to failure of the joint.

Research into adhesive joints has primarily assessed performance based upon ultimate tensile strength [7] [8] and investigations in strength improvements through parametric geometry changes [9–11]. Little consideration has been given to experimentally analysing the complex strain distributions generated with the joint, and their influence on the formation of damage within the composite material in the weak through-thickness direction. In the present paper Digital Image Correlation (DIC) is used to evaluate the individual strain components generated within the joint up to and including failure. Strain fields are examined at the root of the discontinuity in the joint to provide detailed, data-rich, measurement of the developing strain fields. Data gathered from the present investigation is used to observe changes in the fundamental material and structural responses, which are critical to the formation of damage in the complex composite structures. Importantly for designers and engineers, the data can be used to validate numerical models which can be employed to efficiently represent the developing stresses and strains in complex composite structural joints.

The response of the bonded assembly is also investigated under high rate loading due to the high incidence of dynamic loading events in marine structures during operation, as shown by Manganelli’s study of bow accelerations in 50ft & 60ft global race yachts [12]. Dynamic loading incidences due to heavy seaways, ship motions or human factors, such as impacts, produce very fast impulse loading of the structure [13–15]. These dynamic incidences result in rapidly changing stresses, [16] increasing the potential for significant damage to the structure [17]. Under these high-rate loading incidences both metallic and composite materials display rate-dependent material properties. Metallic structures exhibit an increase in stiffness and strength due to plasticity and dislocation dynamics [18], and composites display an increase in strength due to viscoelastic effects within the matrix [19]. Investigation of joints has observed changes in the response of the adhesive used within the bonded joints [20–22] as well as the overall structural dynamics of bonded assemblies in tension [23], [24], compression [25] and shear [26], [27].

In the present paper, testing is conducted both quasi-statically and at high rate, observing changes in the joint behaviour between conditions. High speed cameras are used to provide high temporal resolution DIC analysis of the developing strain fields within the joint structure. Changes in the joint strength and strain distribution are identified, providing a better understanding of the dynamic, real-world, behaviour of bonded composite joints. Knowledge of the dynamic failure behaviour can be used to improve joint designs, and be engineered to maximise in-service performance whilst minimising the initiation of damage.

Digital Image Correlation

Digital image correlation is a full-field optical white light technique based on the comparison of images before, during and after the deformation of a test specimen. To facilitate the correlation a stochastic speckle pattern is applied to the specimen surface, providing random grey level variation across the image. An image correlation algorithm is used to identify areas of matching pattern between images [28–31]. The position where the correlation function value is maximised in the deformed image corresponds to the movement of the pattern during deformation. The images of the speckled specimen are divided into a grid of smaller interrogation cells, or subsets. The correlation between images is undertaken for each subset, creating a full-field array of displacement vector data points across the image. A central differences approach is used to determine the full-field strains from the deformation results. A schematic of the correlation process can be seen in Fig 2. The spatial resolution and accuracy of the displacements are limited by the total number of pixels within the image. The spatial resolution of the data is maximised by reducing the size of the subsets, but as the interrogation cell size decreases, the uncertainty in the strain measurement increases due to a reduction in the number of features to track within the subset [32]. A more detailed explanation of the digital image correlation process and discussion of alternative correlation approaches can be found in literature presented by Pan [30], Sutton [28].

FIG 2

Joint structure

A single lap joint (SLJ) was selected for analysis due to its simple construction, large geometric discontinuity and high through-thickness loading occurring between adherends. The joint was constructed from four layers of 800g/m^2 unidirectional and 14 layers of

450g/m^2 chopped strand mat (CSM) glass fibre in a [CSM_7 90_4 CSM_7] layup using Gurit Prime 20 LV epoxy resin and the resin infusion process. The SLJ specimen is shown Fig 3a); it is 25 mm wide with an adherend overlap length of 25 mm. The adherends had a total length of 150 mm with a 50 mm tapered end tab design. Araldite 2015, a toughened structural epoxy adhesive, was used to bond the adherends together. The layup selected created a laminate with comparable material and thickness to many marine laminates. The surface of the laminate which lay against the flat mould tooling during manufacture was used as the bonding surfaces in the joint. The specimens were manufactured by bonding the adherends together in one 400mm wide joint, before cutting it thinner joints for testing. This method minimises misalignment of the adherends during assembly and provides greater control over the symmetry of the joint, both of which create more repeatable joints for testing.

The surfaces of the adherends were prepared for bonding by abrading the bonding areas with P120 sandpaper and a flat sanding block to remove the resin rich surface layers of the material and generate a clean surface for bonding. The abraded surfaces were cleaned with acetone to remove any dirt or grease. Pressure was applied to the bond area during curing using five 5 kg lab weights; ensuring good contact between the adherends and the adhesive. The joint assembly was post cured at 80^{o}C for 1hr as per the manufacture's data sheet instructions to maximise the shear strength of the adhesive. Thick layers of dissimilar material in the laminate provide sufficient thickness across each material layer for a large number of data points to be captured in the strain analysis. An image of the layered joint structure is shown in Fig 3b).

The SLJ layup and overlap length were designed to ensure that the response of the joint in the through-thickness direction is adequately captured using the optics and cameras available. Adhesive spew fillets were removed during construction to artificially increase the peel strain in the thick, stiff adherends. Although not perfectly representative of joint geometries used in current marine structures, evaluation of the SLJ demonstrates the potential of the full-field, non-contact DIC technique to analyse complex composite structures. The single lap joint has also been extensively tested and modelled in literature [33] [34] [35] [36], which provides confidence in the experimental methodology and the results discussed later in the paper. Using this joint geometry as a demonstrator gives confidence in the experimental methodology for evaluating complex structures. It shows the technique to be a powerful analysis tool for structures where there is little knowledge or previous investigations of the material and structural responses, such as in large marine structures.

FIG 3

SLJ quasi-static analysis

The SLJ was initially tested quasi-statically to establish a baseline joint response, against which the effects of dynamic loading are compared. The joint was mounted in an Instron 5569 electromechanical test machine and loaded at 2 mm / min up to failure. A 16 MP 14 bit monochromatic LaVision Imager pro X camera fitted with a Sigma 105 mm macro lens was used to image the specimen with an image resolution of 142 pixels / mm at 5 Hz. Illumination was provided by a LED ring flash light mounted onto the lens, delivering consistent cold lighting of the specimen. The stochastic speckle pattern, which the correlation algorithm uses to calculate deformation vectors, was applied using RS components matt black aerosol, fitted with a needle cap, onto a white background painted onto the specimen. The pattern properties were matched to the resolution of the image, minimising errors in the correlation. The sequence of images was processed using the LaVision Davis 8.0 correlation software, with a subset size of 75 x 75 pixels and a step size of 25 pixels, delivering a spatial resolution of approximately 5 data points / mm.

Figs 4a-c) show a detailed view of the evolving peel strains, ε_x, within the joint loaded at 1.5, 3 and 4.7 kN respectively. Peel strain concentrations form at the root of the geometric discontinuities in the CSM layers either side of the adhesive layer between adherends. These concentrations form due to the internal bending moments created from the load path eccentricity and become larger with greater applied load. The peel strain is greatest at the free end of the adherends, where the structure is least constrained, experiencing the greatest deformations. The bending and rotation of the joint during deformation generates a band of high interfacial peel strain between the CSM and 90° materials around the discontinuity in the adherend adjacent to the free end. The localised strains, generated at the discontinuity, result in the initiation of a crack and the propagation of damage downwards in to the joint, (see Fig 4c), and final joint failure at 4.8 kN. The white contours in the figure are areas of very high strain in the adhesive where the colour scale is saturated. This scale was chosen in order to observe the strain distributions in the composite adherends which is the objective of the paper.

Figs 5a)-c) show the development of the shear strains within the joint at the same load intervals as Fig 4. As expected, the largest shear strain is experienced within the adhesive layer, as shear is the primarily load transfer mechanism between the inner and outer adherends. A symmetrical shear strain distribution is observed, peaking towards the discontinuity. The bending of the adherends is observed to generate greater shear strains in the face sheet CSM material compared to the central 90^{o} material, contributing to the high, damage inducing, strain field at the root of the discontinuity. A plot of the axial strain distributions in the joint are shown in Figs 6a)-c), identifying a non-uniform deformation field across the joint due to the load transfer between adherends. A zero displacement condition can also be observed at the free end of the adherends.

FIG 4

FIG 5

FIG 6

Analysis using the DIC technique provides a detailed and complimentary view of the localised peel and shear strain distributions generated within the joint. High spatial resolution full-field data is gathered, identifying the global and local material behaviours within the joint, and the influence these high strain regions have at the discontinuity on the initiation of failure. The strain distributions in Figs 4, 5 and 6 demonstrate that the relatively simple discontinuity between components results in very complex, inter-dependent strain distributions within the joint. The detail of these critical localised strain distributions would not be obtained using traditional single point measurement techniques such as strain gauges. The observed strain distributions agree with existing numerical models of single lap joints, such as the peel and shear distributions along the bondline evaluated by Goland and Reisner [36]. The shear, peel and axial strain distributions also show good agreement with those seen by Kumar et al [35] and Tsai and Morton [37] of composite single lap joints, giving confidence that the experimental methodology is accurately observing the load transfer mechanics between adherends in the joint. The localised peel and shear strains identified at the root of the discontinuity play a significant role in the development of damage and the control of ultimate joint failure, providing an initiation site for damage in the strain critical brittle epoxy matrix leading to ultimate joint failure. With the current spatial, and temporal, resolutions there is insufficient detail to resolve the initiation and propagation behaviour around this damage critical region and needs to be investigated further.

To improve the temporal resolution of the data, quasi-static tests were conducted using the same test procedure with a 10 bit Photron SA5 high speed camera. The high speed camera provides the capability to capture the fast initiation and development of damage within the joint up to an including failure. Images were recorded at 1000 Hz with an image resolution of 464 x 384 pixels. The image size is much smaller than achieved previously with the 16 MP LaVision Imager pro-x camera due to limits in the on board camera memory and the high speed imaging technology. To compensate, optics are used to increase the magnification of the image, increasing the number of pixels per millimetre in the image. This provides an image with a high spatial resolution at the expense of reducing the size of the area of interest for the analysis. An area of interest 6.2 mm x 5.1 mm was imaged at the root of the discontinuity between the adherends, where damage was observed in Figs 4b) and 4c) to initiate and propagate. A sigma 105 mm macro lens was attached to the Photron SA5 producing an image resolution of 75 pixels / mm, approximately half than that of the initial analysis shown in Figs 4 & 5, due to the smaller sensor size of the high speed camera. The image sequence was analysed with a subset size of 69 x 69 pixels and step size of 20 pixels, producing a spatial resolution of approximately 4 data points / mm. Similar experimental methods have been used to analyse small areas of interest around the root of the discontinuity between adherends in a double butt strap joint with high confidence [38].

Fig 7 shows the a) axial, b) shear and c) peel strain distributions within the joint at 2.7 kN. Although the image resolution with the high speed camera is lower than the previous analysis, analysing the joint with a high temporal resolution is very important in establishing an understanding of the rapid crack growth behaviour within the joint. These two high spatial and temporal resolution data sets complement each other, providing a reference against which the high rate testing results can be evaluated. Fig 7a) shows higher axial strain in the constrained adherend on the left compared to the free adherend on the right, identifying the free adherend to be lightly loaded. The axial strain field provides a quantitative visualisation of the differential extension between adherends in the single lap joint due to the different boundary conditions within the free end of the adherend on the right and the highly loaded adherend on the left. As seen in Fig 7b), within the joint the shear strains are greatest within the adhesive layer between adherends at the discontinuity, decreasing rapidly away from the adhesive into the surrounding CSM material. Peel strains shown in Fig 7c), are concentrated in the right hand adherend close to the free end, where load eccentricity is at its greatest, reducing quickly away from the discontinuity.

Fig 8 shows data for an increased load of 3.1 kN; here the peel and shear strain distributions develop into distinct, yet inter-dependent features. Analysis of the shear strains identifies a non-uniform distribution across the thickness of the adhesive layer, generating higher shear strains closer to the interface between the adhesive and the adherend on the right, propagating into the CSM face sheets, Fig 8b). The peel strain in Fig 8c) is greatest adjacent to the region of high shear strain at the interface between the adhesive and right hand adherend. The position of these concentrations indicates a coupling between the through-thickness and shear material responses at the interface resulting from the load transfer across the adhesive into the adherend. A similar localisation of the strains along the interface was observed by Ruiz [39] using high magnification Moiré interferometry. The high strain along the interface is suspected to feature heavily in the initiation and propagation of damage.

The first visual signs of damage in the joint can be observed at 3.1 kN from the raw images. A very small 0.13 mm crack forms at the root of the discontinuity at the interface between the adhesive and the left hand, constrained, adherend. As this crack is very small it is not easily discerned in the images. For the purpose of illustration, Figure 9a) shows the crack at 3.8 kN when it is more clearly visible in the image. Shear strains in the adhesive layer are 1.8% just prior to the crack initiation. The peel strain is much lower; between 0.15-0.2% and 0.5% axial strain in the left hand adherend. The failure site is located within the left hand adherend, where the local peel and shear strains are lower than along the interface as identified in Fig 4c. This suggests that the initiation of damage is dominated by peel and not shear strain. The severe geometric discontinuity at this location is also suspected to influence this damage in the high axially loaded adherend.

The joint demonstrates significant residual strength and damage tolerance, with the load trace largely unaffected by the steadily growing crack up to a length of 0.4 mm at 4.5 kN. Shortly after exceeding 4.5 kN a critical crack length is reached and the crack growth becomes rapid and unsteady leading to the final failure of the joint. The evolution of the crack from stable to unstable behaviour is aided by high peel and shear strains which form ahead of the crack tip. These high strains generate micro cracks ahead of the crack tip in the adhesive layer. Above 4.5 kN these micro cracks coalesce, forming a large single crack, rapidly increasing the crack growth speed, up to a maximum crack length of 3.2 mm as shown in Fig 9b) after which joint failure occurs,.

The strain distributions obtained from this investigation form a comprehensive baseline, against which testing at high speed, representative of dynamic marine loading conditions, are evaluated. The full-field DIC analysis is shown to be an effective tool for the evaluation of the complex spatial and temporal behaviours occurring within the laminated structure of the composite joint. The data identifies localised phenomenon at the root of the discontinuity to be critical to the damage initiation and tolerance of the composite structure.

FIG 7

FIG 8

FIG 9

SLJ High strain rate analysis

To date, the majority of high strain rate testing of composite materials and bonded components have used a split Hopkinson pressure bar, imparting strain rates of up to 10^4 s^{-1}. To achieve a constant strain rate loading it is usually the case that test coupon is relatively small, hence limiting the type of structure and material that can be tested. Drop test rigs and Charpy impact test rigs have also been used to assess strain rate sensitivity of adhesively boned coupons under impact [40] and tension [41], [42], but are only capable of strain rates up to 10 s^{-1}. In this work an Instron VHS 80/20 servo hydraulic test machine, capable of actuator displacement speeds up to 20 m/s, specially adapted for composite materials is utilised. The geometry of the specimens used in this machine are of similar size as those as defined by British (BS), International (ISO) and American (ASTM) standards at quasi-static rates. The set-up of this machine provides results which are directly comparable between the high speed and quasi-static test cases. There is a large enclosure around the machine allowing good optical access of the specimen with high speed cameras as it is loaded. The machine operates by the controlled single shot release of an oil reservoir held at 280 bar through a control valve. The first 100 mm of the actuator displacement is within a hollow 'slack adapter' system attached to the bottom of the specimen, see Fig 10. This allows the acceleration of the actuator up to constant velocity, removing any inertial loading from the specimen. At the end of this initial displacement the actuator engages the end of the slack adapter tube, loading the specimen, as shown in Fig 10. The speed and travel of the actuator allows for testing at strain rates up to 10^2 s^{-1}. The load is measured using a 100 kN Kistler piezo-electric load cell sampled at 3 MHz. A TTL pulse generator is used to synchronise the data and image capture between the test machine and the Photron SA5 high speed camera during the failure event, triggered from the displacement of the slack adapter system just prior to engaging the loading mechanism.

FIG 10

High speed testing was conducted with an actuator velocity of 2.5 m/s. This loading velocity sits within the range of common slamming impact velocities found by Manganelli of for a 50 foot racing yacht during a circumnavigation of the globe [15]. An area measuring 12 mm x 8.9 mm around the root of the discontinuity was imaged using the Photron SA5 camera. Images were recorded with a temporal resolution of 25 kHz and an image resolution of 600 x 448 pixels. The failure of the joint occurs rapidly, approximately 1 millisecond, presenting a significant challenge in observing the development of the strain fields and damage within the joint up to failure, as very few images are recorded during the loading and failure event.

FIG 11

FIG 12

Fig 11 shows the load trace from 4 specimens tested in the Instron VHS machine. The joints load steadily up to approximately 6 kN, above which there are small fluctuations in the load trace associated with the growth of damage up to final failure at approximately 9 kN. The failure load during the quasi-static analysis was 4.5 kN, showing a 100% increase in the failure load of the joints due to the increased loading rate. This is a significant change in joint strength, and is greater than reported previously in similar testing of adhesives [43], composite double butt strap joints [23] or single lap joints [42], which used composite layups with 0^o, 90^o, 45^o and woven $0/90^o$ adherend face sheets. This suggests that the increase in strength may be due to the behaviour of the CSM face sheet material, and its influence on the failure mechanisms within the joint. A noticeable change in the failure surfaces for the joint is observed between the two different loading regimes. At the quasi-static rate the failure surface shows the crack growth to occur along the interface between the adhesive and the composite adherend, with practically no crack growth into the composite adherend, as shown in Fig 12a). At the elevated loading rate a different failure surface is observed, see Fig 12b), which shows fibre-tear failure between adherends. This indicates that the crack has grown within the adherend rather than just at the adhesive interface, resulting in the violent failure surface observed. The consistent and dramatic change in the failure surfaces at the high loading rate suggests a change in the behaviour associated with the increase in ultimate joint strength through greater interaction between the CSM face sheet and the crack front. This crack/fibre interaction is apparent from the variation in the load traces of the four specimens in Fig 11 above 5.2 kN, indicating the variable development of damage within the joint.

Analysis of the developing strain fields using DIC from the high speed imaging was used to evaluate the behaviour responsible for the changes in joint strength. The high speed images were processed with a subset size of 49 x 49 pixels and a step size of 15 pixels, producing a spatial resolution of 3.3 data points / mm. this produces data with a very similar to that of the magnified quasi-static failure analysis in Fig 7. Inspection of the high speed image sequence shows damage to occur at the interface between the right hand adherend and the adhesive layer at the root of the discontinuity, the same location in the joint as observed in the quasi-static analysis using the high speed camera. The initial damage occurs very quickly, appearing in less than 1/25000th of a second between two images at 4.7 kN and 5.2 kN, which is double the load of that in the quasi-static tests. Fig 13 shows the strain fields within the joint loaded at 4.7 kN, prior to any visual indication of damage in the joint. Prior to the initiation of damage in the joint at approximately 50% of the failure load, the shear and axial strains next to the discontinuity are very similar to those in the quasi-static analysis also close to 50% failure load At the root of the discontinuity the shear and axial strains reach a maximum of 1.1%, and 0.35% respectively at the interface between the adhesive layer and the right hand adherend. Very small peel strains, with a low signal to noise ratio are observed, due to the low spatial resolution of the image, resulting in a poor correlation of the through-thickness strains, limiting the analysis of the damage initiation event. The similarity of the strains prior to damage at quasi-static and high speed loading shows that the initiation of damage is predominantly a strain critical response within brittle epoxy matrix of the right hand adherend at the root of the discontinuity, where the geometric discontinuity is the most severe, and the stress is concentrated locally in the adherend.

The loading curve in Fig 13 increases to well above 5.2 kN, maintaining significant load carrying capability while damage propagates, up to final failure at 9.7 kN. The strain fields at 8 kN show high axial strain in the right hand adherend during the propagation of damage within the joint. Axial strain up to 0.65% forms within the undamaged CSM material in the right hand adherend. Transverse cracking of the epoxy matrix is also visible in the 90^o fibres in the middle of the adherend due to the high axial strain in the adherend. The axial strains in the CSM material identifies the continued load transfer between adherends in the damaged condition provided by fibre bridging of the CSM layers across the crack front between adherends. This agrees with the very violent failure surfaces, which show fibres pulled out of the adherend aligned parallel to the direction of load. The CSM material also appears to provide some crack blunting properties, reducing the propagation speed in the joint, as identified by the large increase in ultimate strength compared to the results in literature discussed earlier.

Testing at high speed shows a large increase in the ultimate strength of the joint, indicating a strengthening due to the viscoelastic behaviour of the material. Analysis of the strain fields shows the initiation of damage occur at similar strain levels between both loading rates tested, at approximately 50% of the final failure load. The initiation of damage therefore is a strain critical event, independent of loading rate and strengthening of the material. The strain distributions show very complex load transfer behaviour around the joint, exhibiting significant mixed mode loading, and coupled material response around the discontinuity. As a result, the strain rate sensitivity of the joint strength cannot be thought of as a single global response, but is a function of many different local material and dynamic behaviour in the neighbourhood of the crack-tip. Full analysis of these material and damage mechanics sensitivities ultimately is not possible with the current equipment, due to severe limitations in the spatial and temporal resolutions of the high speed cameras available. As a result a comprehensive comparison of the material behaviours between loading rates cannot be made.

Although limited in resolution due to the currently available hardware, important results have been obtained. A large strengthening effect was observed due to the response of the CSM face sheet material. The initiation of damage did not form in the area of greatest peel and shear strains, but instead was observed to be a strain critical response within the adherend at the root of the discontinuity, where the geometric discontinuity is the most severe and the stress most concentrated. The complexity of the behaviour identified within the relatively simple single lap joint, demonstrates that the local strain distributions have an important, and often inter-dependent, contribution to the joint strength. Typically the joint geometries and loadings regimes in marine structures are a lot more complex, attaching multiple components, containing multiple discontinuities, for which there is no hope for a closed form solution. Therefore it is vital that full-field data rich experimental investigations are used to provide a better understanding of the material behaviour and initiation of damage within complex structures such that engineers and designers have confidence in the use of adhesively bonded joints.

FIG 13

Conclusions

Digital Image Correlation was used to establish the component strain distributions within a composite single lap joint tested up to failure. Analysis focused on the root of the discontinuity between adherends where failure initiation is observed. The joint was tested quasi-statically and at high rate, representing the dynamic loading often experienced by marine structures. High speed imaging was used to analyse the developing strains fields associated with damage initiation and growth with a high temporal resolution. Significant residual strength is observed after the initial development of a crack at the root of the discontinuity in the joint at 50% of the final failure load for both load cases. The strains evaluated prior to failure around the geometric discontinuity were very similar for both conditions, identifying the damage initiation to be strain critical at the discontinuity

Significant damage tolerance was demonstrated after the initial development of failure at approximately 50% of the failure load of the joint, and a 100% increase in the ultimate strength of the joint was experience at high strain rate loading. The increases in joint strength between adherends in the matrix dominated loading direction indicate possible viscoelastic strengthening of the epoxy matrix at high strain rate. The behaviour of the CSM face sheet material was seen to have a strongly beneficial effect on the strength of the joint, altering the failure surfaces and indicating interaction between the fibres and the crack front, slowing the crack propagation.

The results show that DIC is a powerful analytical tool for the evaluation of structures and loading scenarios. This is particularly useful for complex composite structures where full knowledge of the material response and loading conditions are not known, leading to inaccurate numerical models and over engineered or inefficient structural design. Increased experimental testing of marine structures will build this knowledge base, allowing the development of numerical models which accurately represent the behaviour and interaction of heterogeneous strain fields and their relation to the damage. With improved knowledge and models, engineers can improve confidence in the structural integrity of adhesively bonded joints, benefiting from the weight savings and structural efficiency improvements they can offer, producing lighter, faster and more efficient marine structures.

[1] P. Goubalt and S. Mayes, “Comparative Analysis of Metal and Composite Materials for the Primary Structures of a Patrol Craft,” *Naval Engineers Journal*, vol. 108, no. 3, pp. 387–397, 1996.

[2] B. A. Brent and S. Brigham, “Joining composite materials - Mechanical or Adhevise?” [Online]. Available: http://strong.groups.et.byu.net/pages/articles/articles/joining2.pdf. [Accessed: 28-Jan-2013].

[3] S. D. Thoppul, J. Finegan, and R. F. Gibson, “Mechanics of mechanically fastened joints in polymer-matrix composite structures - A review,” *Composites Science and Technology*, vol. 69, no. 3–4, pp. 301–329, 2009.

[4] R. W. Messler, “The challenges for joining to keep pace with advancing materials and designs,” *Materials and Design*, vol. 16, pp. 261–269.

[5] F. Campbell, *Structural Composite Materials*. ASM International, 2010, pp. 449–451.

[6] O. Jacobs, K. Friedrich, and K. Schulte, “Fretting fatigue of continuous carbon fibre reinforced polymer composites,” *Wear*, vol. 145, no. 1, pp. 167–188, Apr. 1991.

[7] L. da Silva and R. D Adams, “Techniques to reduce the peel stresses in adhesive joints with composites,” *International Journal of Adhesion and Adhesives*, vol. 27, no. 3, pp. 227–235, Apr. 2007.

[8] T. Keller and T. Vallée, “Adhesively bonded lap joints from pultruded GFRP profiles. Part II: joint strength prediction,” *Composites Part B: Engineering*, vol. 36, no. 4, pp. 341–350, 2005.

[9] R. H. Kaye and M. Heller, “Through-thickness shape optimisation of bonded repairs and lap-joints,” *Journal Of Adhesion*, vol. 22, pp. 7–21, 2002.

[10] T. P. Lang and P. K. Mallick, “Effect of spew geometry on stresses in single lap adhesive joints,” *Journal Of Adhesion*, vol. 18, no. October 1997, pp. 167–177, 1998.

[11] P. Raos, D. Kozak, and M. Lucic, “Stress Strain Analysis of Single Lap Tensile Loaded Adhesive Joints,” in *Proceedings of the 9th International Conference on Numerical Methods in Industrial Forming Processes*, pp. 1093–1098.

[12] P. Manganelli and P. Wilson, “An experimental investigation of slamming on ocean racing yachts,” in *Proceedings of the 15th Chesapeake Sailing Yacht Symposium*, 2001.

[13] T. Allen, M. Battley, P. Casari, B. Kerling, I. Stenius, and J. Westlund, “Structural Responses of High Performance Sailing Yachts to Slamming Loads,” in *11th International Conference on Fast Sea Transportation*, 2011, no. September 2011, pp. 585–592.

[14] E. Lolive, P. Casari, and P. Davies, “Loading rate effects on foam cores for marine sandwich structures,” in *Proceedings of the 7th International Conference on Sandwich Structures*, 2005, pp. 895–903.

[15] P. Manganelli, “Experimental investigation of dynamic loads on offshore racing yachts,” University of Southampton, 2006.

[16] M. Hobbs and P. Manganelli, “Measurment of accelerations and keel loads on canting keel race yachts,” in *RINA Modern Yacht Conference*, 2007.

[17] M. A. Battley, T. Allen, P. Pehrson, I. Stenius, A. Rosen, and N. Zealand, “Effects of panel stiffness on slamming responses of composite hull panels,” in *17th International Conference on Composite Materials ICCM17*, 2009.

[18] R. W. Armstrong and S. M. Walley, “High strain rate properties of metals and alloys,” *International Materials Reviews*, vol. 53, no. 3, pp. 105–128, 2008.

[19] G. C. Jacob, J. M. Starbuck, J. F. Fellers, S. Simunovic, and R. G. Boeman, “Strain Rate Effects on the Mechanical Properties of Polymer Composite Materials,” *Polymer*, 2009.

[20] T. Iwamoto, T. Nagai, and T. Sawa, “Experimental and computational investigations on strain rate sensitivity and deformation behavior of bulk materials made of epoxy resin structural adhesive,” *International Journal of Solids and Structures*, vol. 47, no. 2, pp. 175–185, 2010.

[21] M. A. Martınez, I. S. Chocron, J. Rodrı, V. Sanchez, and L. A. Sastre, “Confined compression of elastic adhesives at high rates of strain,” *Journal Of Adhesion*, vol. 18, pp. 375–383, 1998.

[22] L. Ã. Goglio, L. Peroni, M. Peroni, and M. Rossetto, “High strain-rate compression and tension behaviour of an epoxy bi-component adhesive,” *Journal Of Adhesion*, vol. 28, pp. 329–339, 2008.

[23] O. Essersi, M. Tarfaoui, S. W. Boyd, F. Meraghni, and R. A. Shenoi, “Dynamic study of adhesively bonded double lap composite joints,” in *17th International Conference on Composite Materials*, 2009.

[24] L. Zachary and C. Burger, “Dynamic wave propagation in a single lap joint,” *Experimental Mechanics*, vol. 20, no. 5, pp. 162–166, May 1980.

[25] G. Challita and R. Othman, “International Journal of Adhesion & Adhesives Finite-element analysis of SHPB tests on double-lap adhesive joints,” *International Journal of Adhesion and Adhesives*, vol. 30, no. 4, pp. 236–244, 2010.

[26] S. Raykhere, P. Kumar, R. K. Singh, and V. Parameswaran, “Dynamic shear strength of adhesive joints made of metallic and composite adherents,” *Materials and Design*, vol. 31, no. 4, pp. 2102–2109, 2011.

[27] C. Sato and K. Ikegami, “Dynamic deformation of lap joints and scarf joints under impact loads,” *Journal Of Adhesion*, vol. 20, pp. 17–25, 2000.

[28] M. A. Sutton, J.-J. Orteu, and H. W. Schreier, *Image Correlation for Shape, Motion and Deformation Measurements: Basic Concepts,Theory and Applications*. 2009.

[29] B. Pan, "Recent Progress in Digital Image Correlation," *Experimental Mechanics*, Nov. 2010.

[30] B. Pan, K. Qian, H. Xie, and A. Asundi, "Two-dimensional digital image correlation for in-plane displacement and strain measurement: a review," *Measurement Science and Technology*, vol. 20, no. 6, p. 062001, Jun. 2009.

[31] F. Hild and S. Roux, "Digital Image Correlation: from Displacement Measurement to Identification of Elastic Properties - a Review," *Strain*, vol. 42, no. 2, pp. 69–80, May 2006.

[32] K. Triconnet, K. Derrien, F. Hild, and D. Baptiste, "Parameter choice for optimized digital image correlation," *Optics and Lasers in Engineering*, vol. 47, no. 6, pp. 728–737, Jun. 2009.

[33] A. J. Comer, K. B. Katnam, W. F. Stanley, and T. M. Young, "Characterising the behaviour of composite single lap bonded joints using digital image correlation," *International Journal of Adhesion and Adhesives*, vol. 40, pp. 215–223, Jan. 2013.

[34] M. Y. Tsai and J. Morton, "The effect of a spew fillet on adhesive stress distributions in laminated composite single-lap joints," *Composite Structures*, vol. 32, no. 1–4, pp. 123–131, 1995.

[35] R. V. Kumar, M. Bhat, and C. Murthy, "Experimental analysis of composite single-lap joints using digital image correlation and comparison with theoretical models," *Journal of Reinforced Plastics and Composites*, vol. 32, no. 23, pp. 1858–1876, Aug. 2013.

[36] M. Goland and E. Reissner, "The stresses in cemented joints," *Journal of Applied Mechanics*, vol. 11, pp. 17–27, 1944.

[37] M. Y. Tsai, J. Morton, and F. L. Matthews, "Experimental and Numerical Studies of a Laminated Composite Single-Lap Adhesive Joint," *Journal of Composite Materials*, vol. 29, no. 9, pp. 1254–1275, Jun. 1995.

[38] G. Crammond, S. . Boyd, and J. . Dulieu-Barton, "Evaluating the localised through-thickness load transfer and damage initiation in a composite joint using digital image correlation," *Composites Part A: Applied Science and Manufacturing*, vol. SUBMITTED, 2014.

[39] P. D. Ruiz, F. Jumbo, J. M. Huntley, I. A. Ashcroft, and G. M. Swallowe, "Strain Measurement in the Adhesive Layer of a Bonded Joint Using High Magnification Moire Interferometry," *Experimental Analysis of Nano and Engineering Materials and Structures*. pp. 357–358, 2007.

[40] S.-S. Pang, C. Yang, and Y. Zhao, "Impact response of single-lap composite joints," *Composites Engineering*, vol. 5, no. 8, pp. 1011–1027, Jan. 1995.

[41] L. Ã. Goglio and M. Rossetto, "Impact rupture of structural adhesive joints under different stress combinations," vol. 35, pp. 635–643, 2008.

[42] C. Galliot, J. Rousseau, and G. Verchery, "International Journal of Adhesion & Adhesives Drop weight tensile impact testing of adhesively bonded carbon / epoxy laminate joints," *International Journal of Adhesion and Adhesives*, vol. 35, pp. 68–75, 2012.

[43] B. Revsin and S. . Bodner, "Experiments on the dynamic tensile strength of metals and plastics," *Isreal Journal of Technology*, vol. 7, pp. 485–493, 1969.

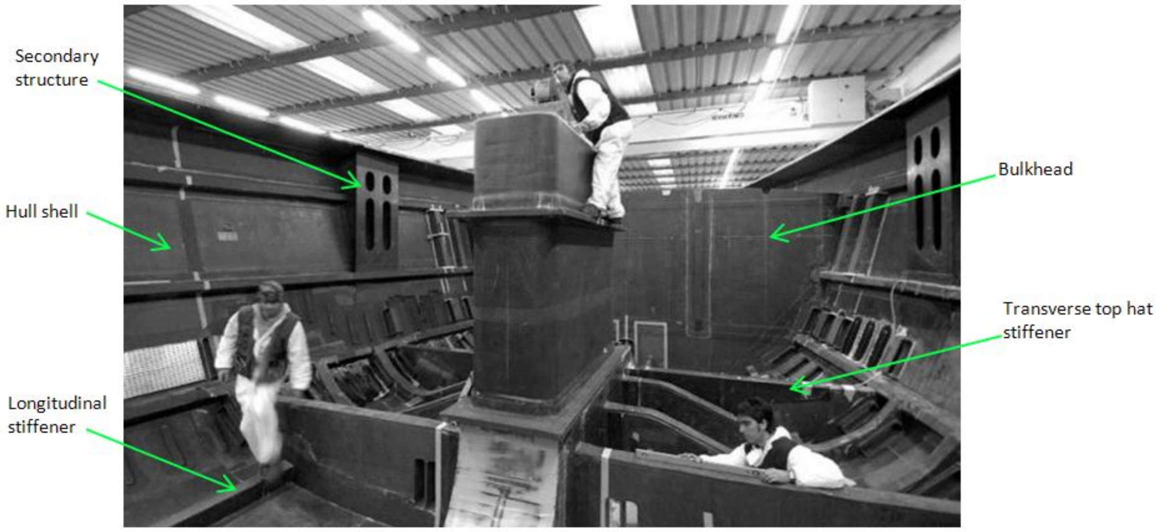

Figure 1: Typical composite structure in yacht hull

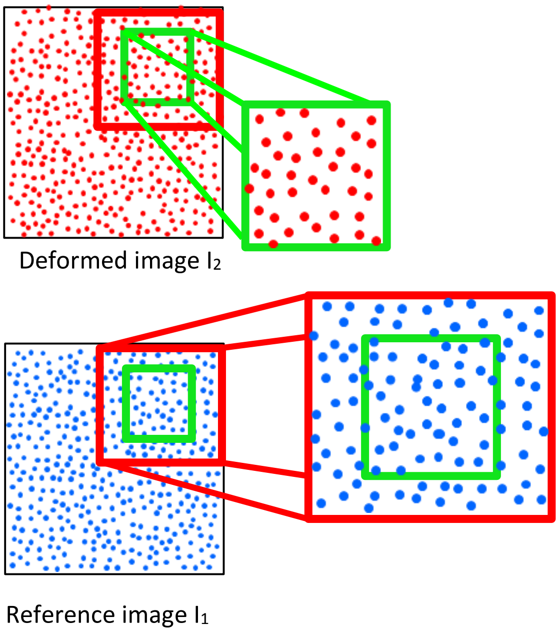

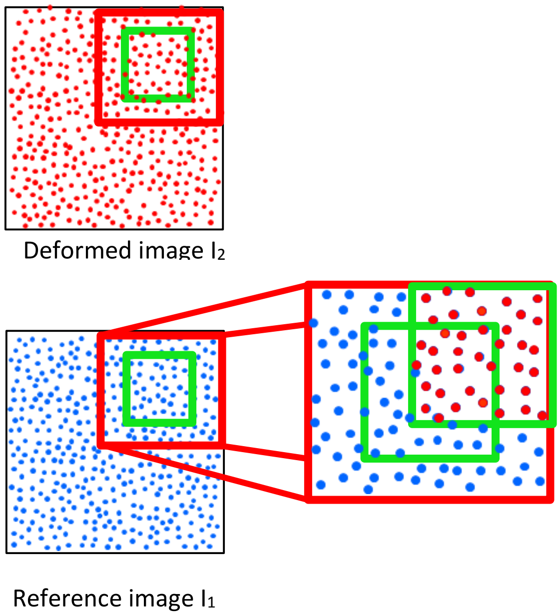

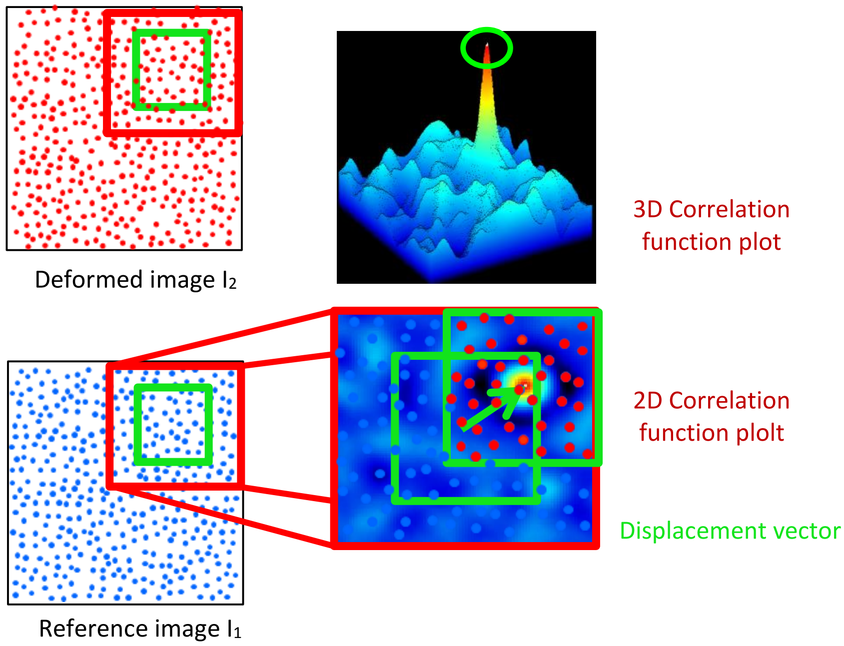

Figure 2: Schematic of the DIC correlation process

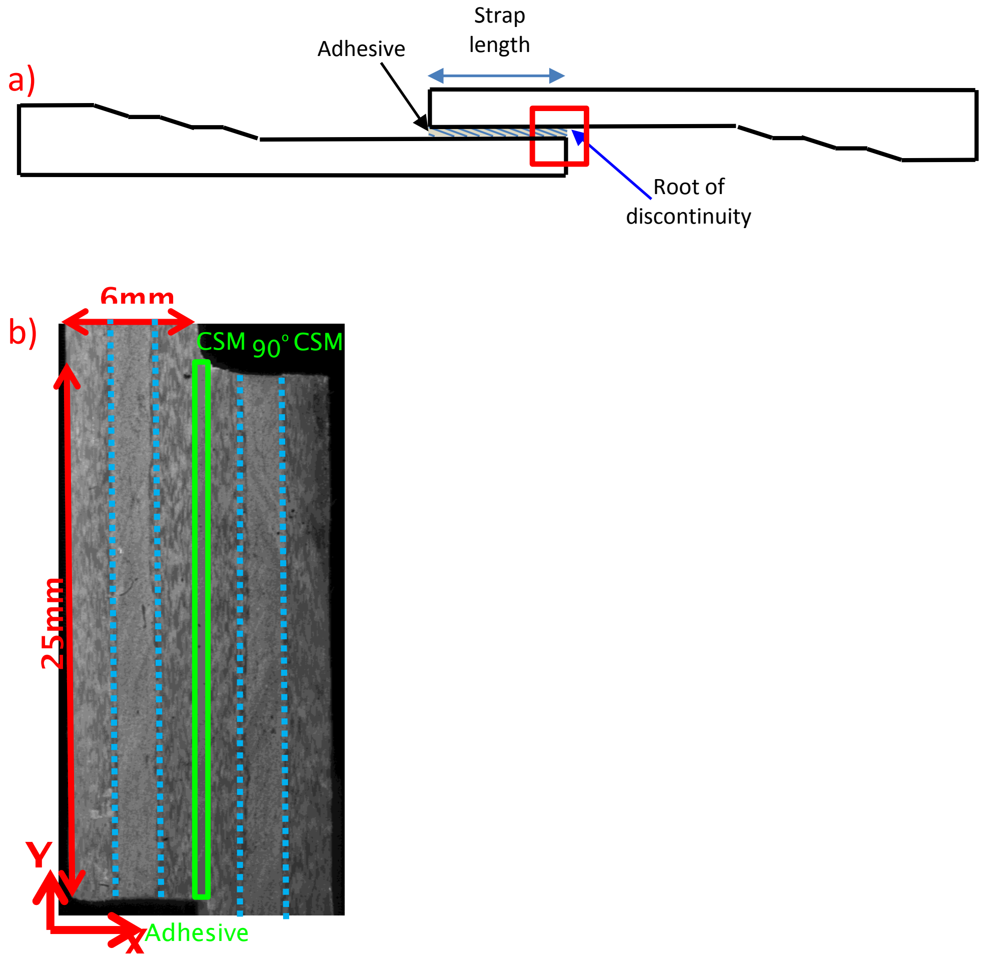

Figure 3:a)Schematic of the single lap joint b) image of the layered composite structure of the joint

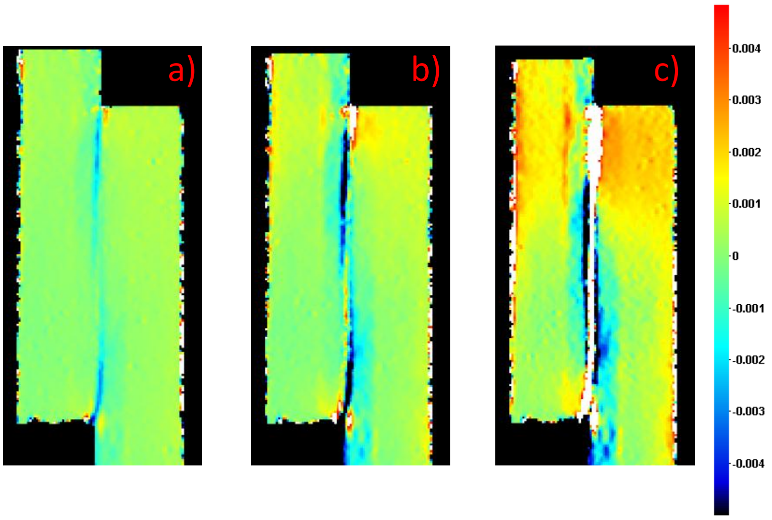

Figure 4: Peel strain within the SLJ at a) 1.5kN b) 3kN c) 4.7kN

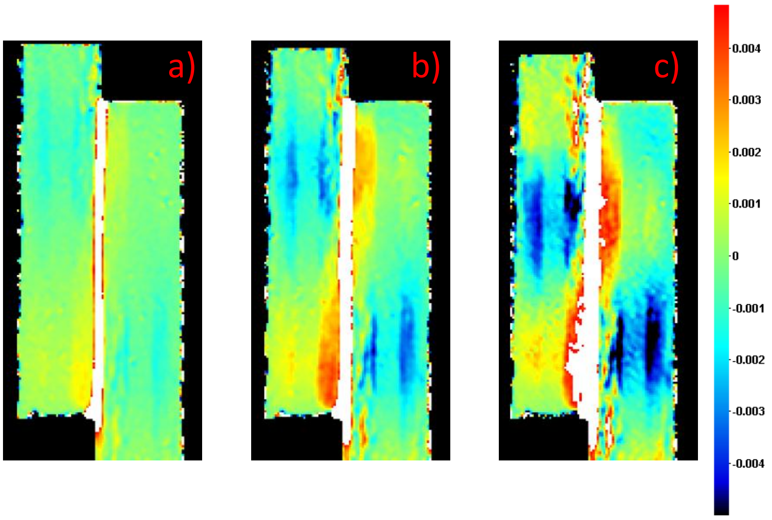

Figure 5: Shear strain within the SLJ at a) 1.5kN b) 3kN c) 4.7kN

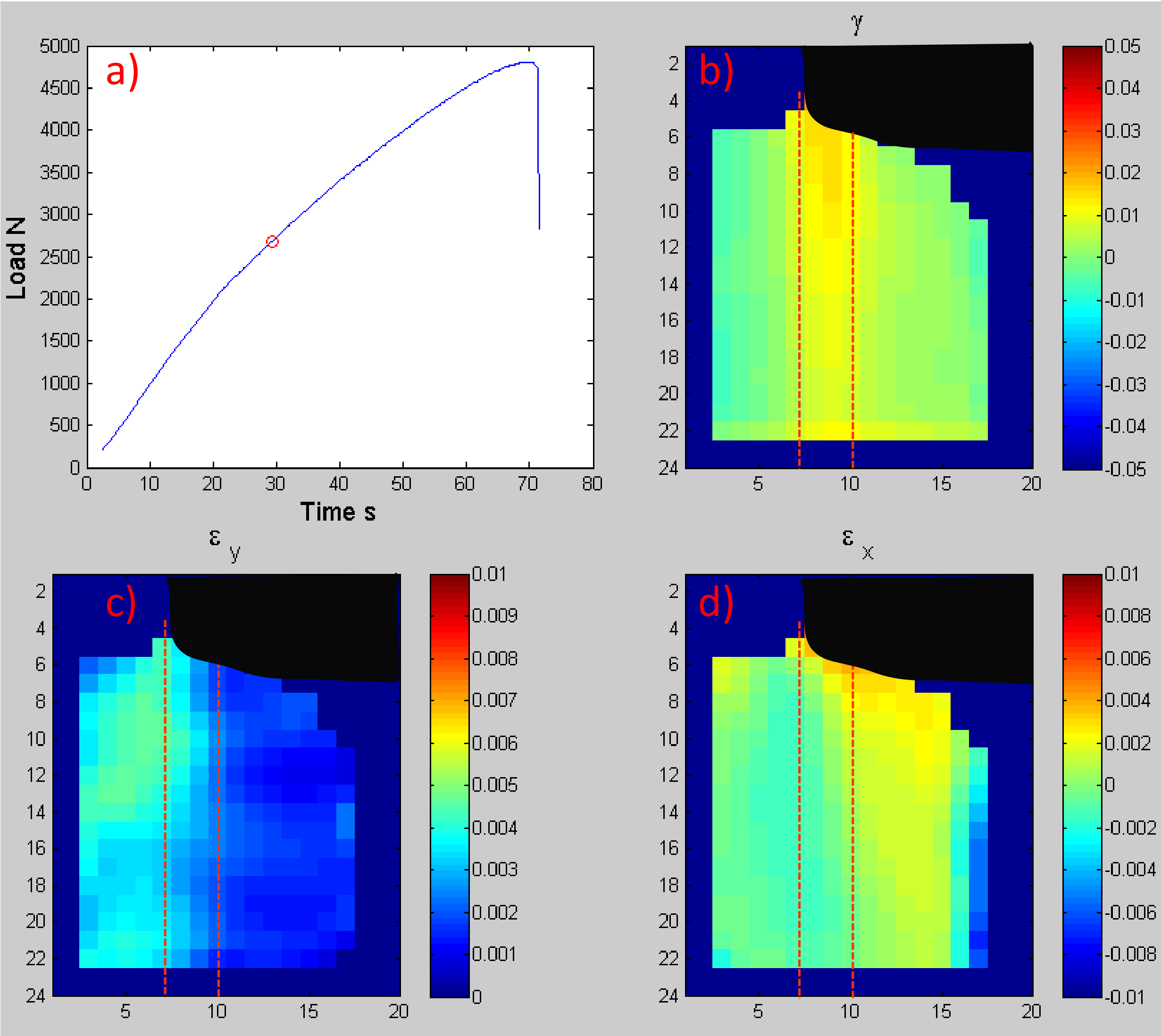

Figure 6: a) joint loading curve. b) shear c) axial d) peel strain fields developed around the discontinuity at 2.7 kN

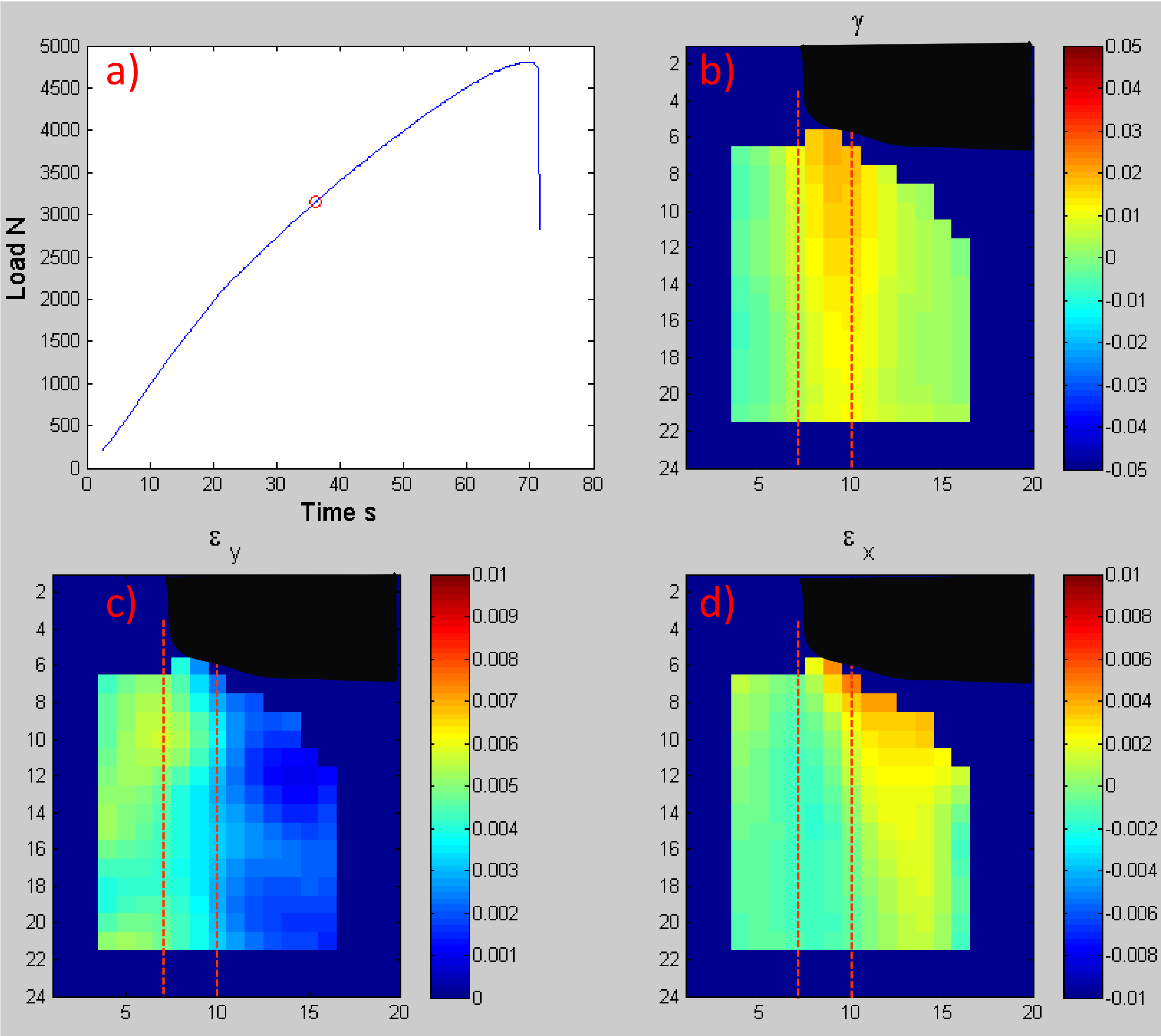

Figure 7: a) joint loading curve. b) shear c) axial d) peel strain fields developed around the discontinuity at 3.1 kN

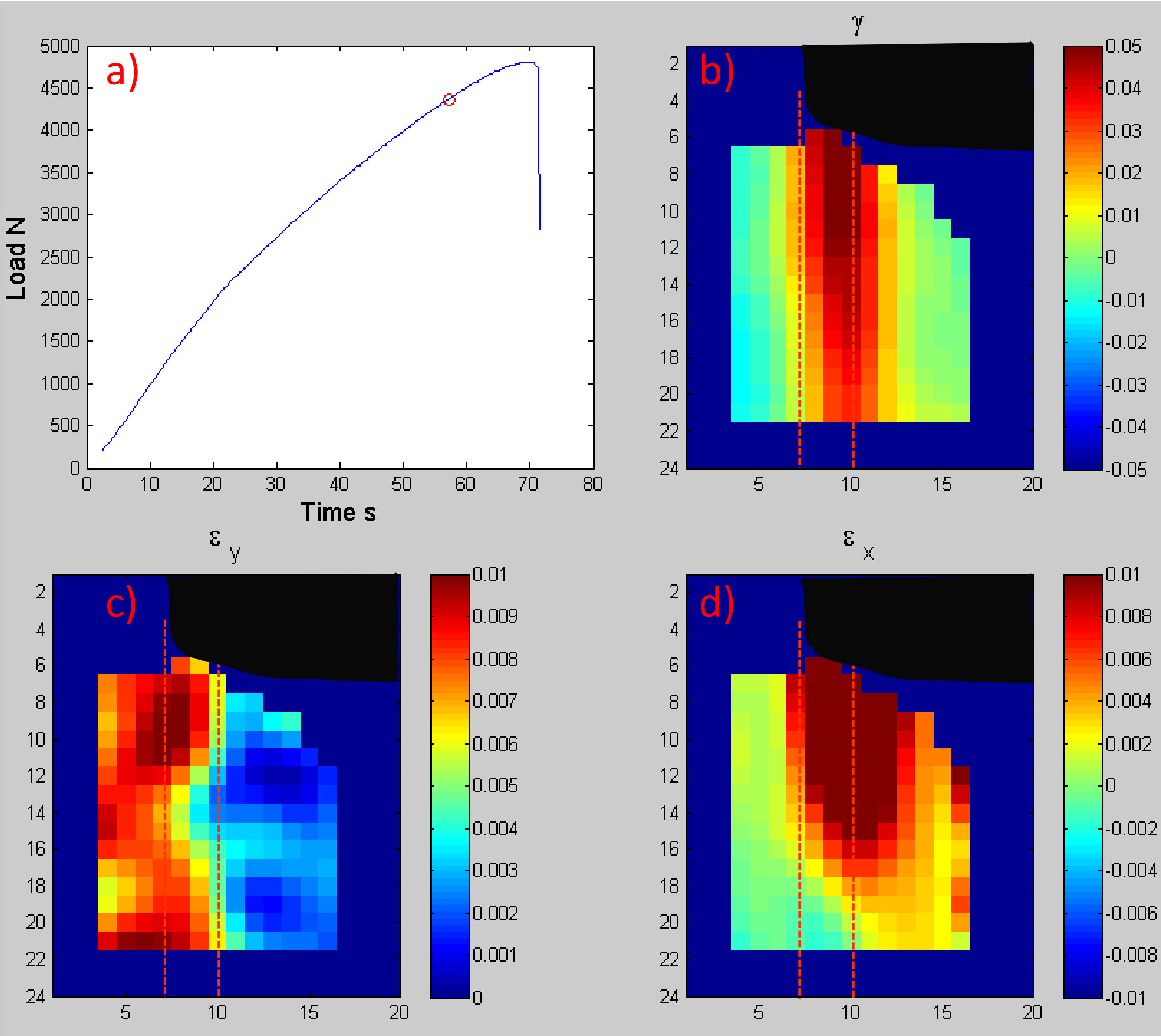

Figure 8: a) joint loading curve. b) shear c) axial d) peel strain fields developed around the discontinuity at 4.4 kN

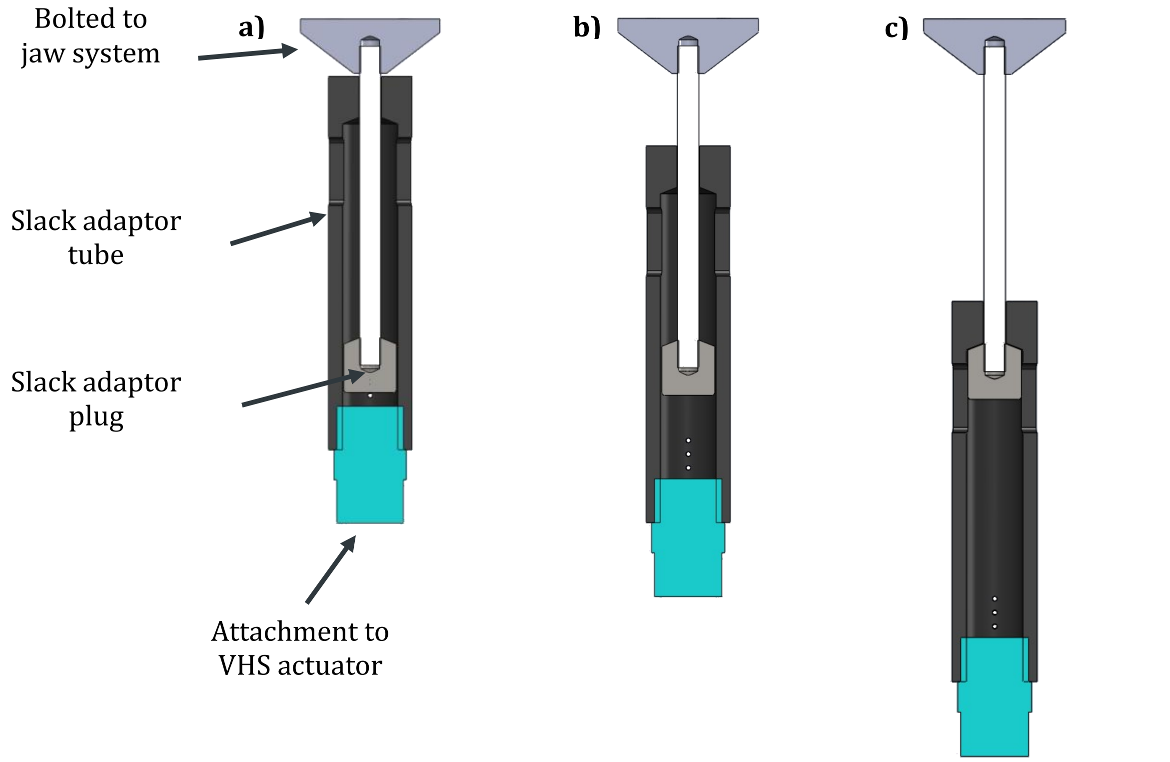

Figure 9: Schematic of the slack adapter system, a) prior to actuator movement, b) during acceleration of the actuator, c) engagement between stack adapter and specimen suring loading at constant velocity

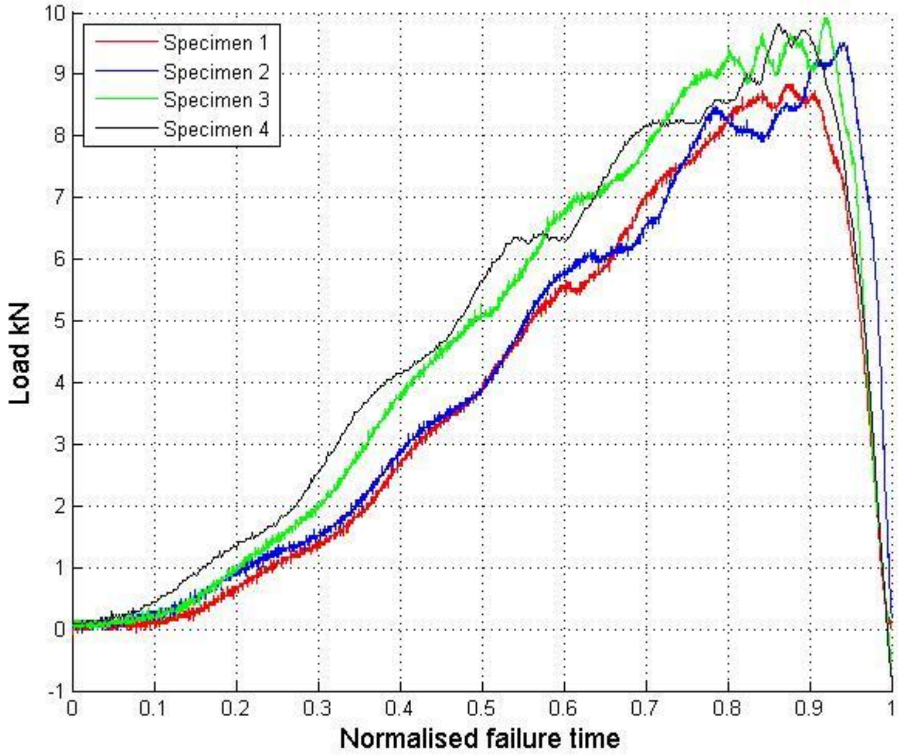

Figure 10: SLJ loading curves at 2.5 m/s

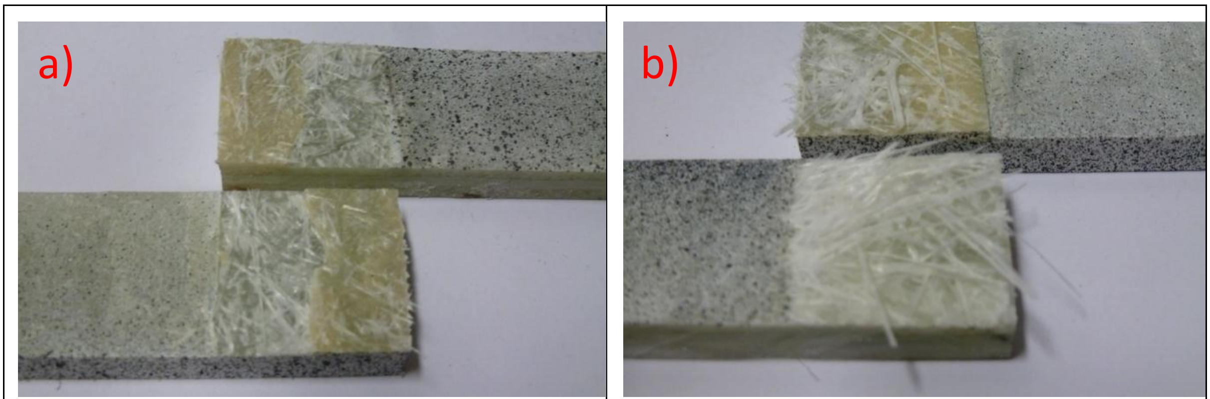

Figure 11: Specimen failure surfaces at a) 2 mm/min b) 2.5 m/s

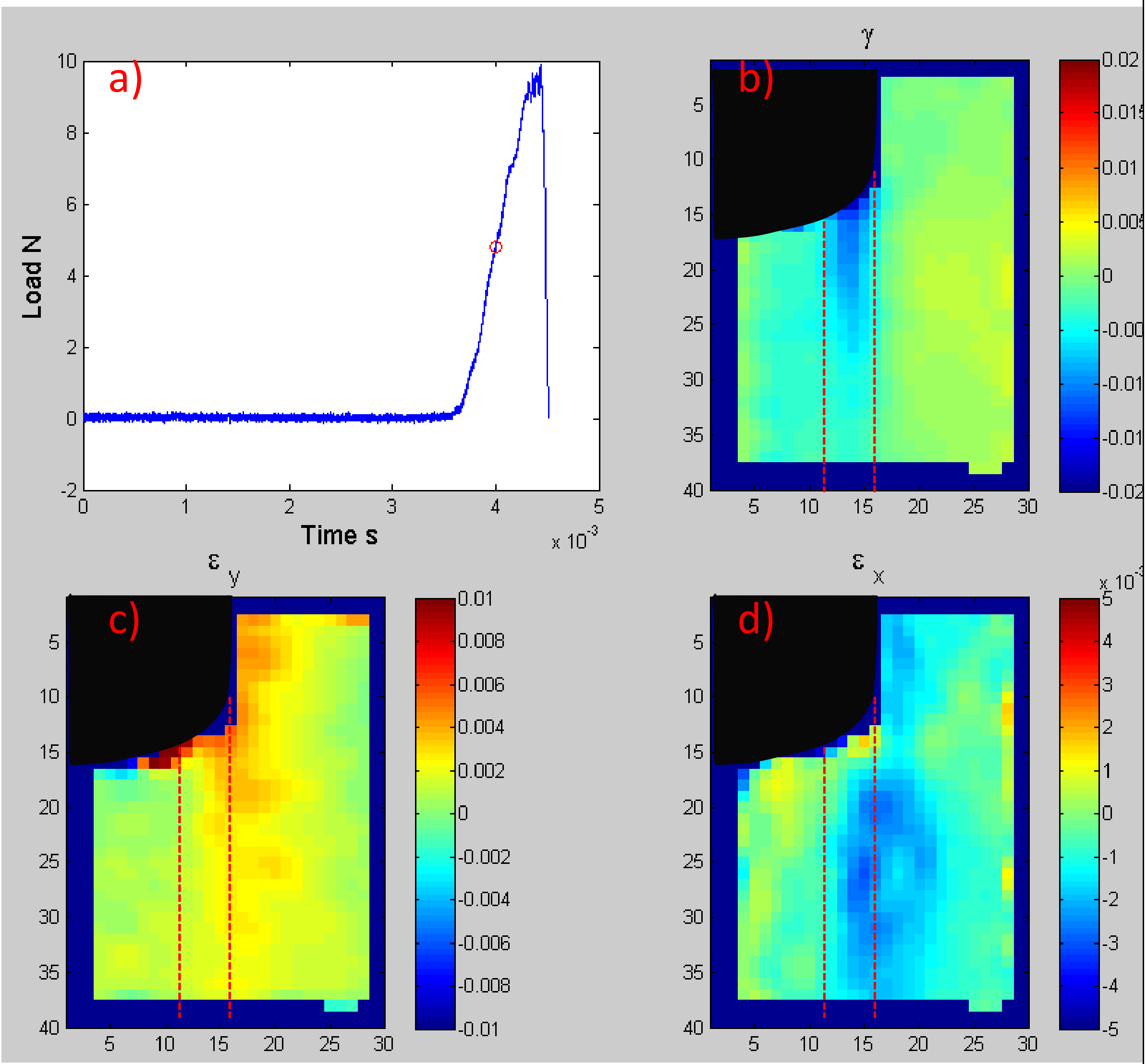

Figure 12: a) joint loading curve. b) shear c) axial d) peel strain fields developed around the discontinuity at 4.7 kN